# *In vivo* reflectance measurement of optical properties, blood oxygenation and motexafin lutetium uptake in canine large bowels, kidneys and prostates

**Michael Solonenko**[1,2,4]**, Rex Cheung**[1,2]**, Theresa M Busch**[2]**,
Alex Kachur**[2]**, Gregory M Griffin**[3]**, Theodore Vulcan**[1,2]**, Timothy C Zhu**[2]**,
Hsing-Wen Wang**[1,2]**, Stephen M Hahn**[2] **and A G Yodh**[1,2]

[1] Department of Physics & Astronomy, University of Pennsylvania, Philadelphia,
PA 19104, USA
[2] Department of Radiation Oncology, University of Pennsylvania, Philadelphia, PA 19104, USA
[3] School of Veterinary Medicine, University of Pennsylvania, Philadelphia, PA 19104, USA

E-mail: yodh@dept.physics.upenn.edu

**Abstract**

Motexafin lutetium (MLu) is a second-generation photosensitizer for photodynamic therapy (PDT) of cancer. We have developed and applied a diffuse optical reflectance spectrometer for *in vivo* measurement of MLu uptake, optical properties, haemoglobin concentration and haemoglobin oxygen saturation in normal canine large bowels, kidneys and prostates.

The probe consists of a broadband fibre-optic-coupled light source and detector fibres placed at various distances from the source fibre to collect reflected light. An analysis based on the diffusion approximation of the photon transport equation was used to recover tissue optical properties from the reflectance measurements. The instrumentation and analysis methods were validated using measurements from homogeneous, highly scattering phantoms with known MLu concentrations. The same techniques were then used to estimate chromophore concentrations of normal canine large bowels, kidneys and prostates.

We estimated (mean (standard deviation)) total haemoglobin concentrations of 119 (25), 340 (92) and 51 (11) $\mu$M in the large bowels, kidneys and prostates of four dogs, respectively; tissue blood oxygen saturations in these same organs were 75 (15), 76 (21) and 74 (16) per cent, respectively. Tissue MLu concentrations (mg l$^{-1}$) were estimated from data taken 3.5 h after injection of a 2 mg kg$^{-1}$ injected dose; data from three dogs gave concentrations of 2.4 (0.4) in large bowels, 6.8 (1.3) in kidneys and 2.2 (1.1) in prostates. The reduced scattering coefficients, $\mu'_s$, estimated for large bowels, kidneys

[4] Present address: Advent Optronics Corporation, 205 Pheasant Run, Newtown, PA 18940, USA.

and prostates at 730 nm were, respectively: 10.1 (1.3), 19.6 (4.0) and 12.7 (0.6) cm$^{-1}$.

We observed significant variability in MLu uptake, tissue scattering and haemoglobin concentration between organs and even between the same organ in different dogs. This class of *in situ* optical property measurement may be desirable to individualize PDT drug and light delivery.

## 1. Introduction

Photodynamic therapy (PDT) is a relatively new cancer therapy that uses non-ionizing photons and a photosensitizer to treat solid tumours and surface malignancies (Dougherty *et al* 1998). The treatment requires administration of a drug, called a photosensitizer. Visible light is then used to excite the photosensitizer. Photoexcitation initiates a cascade of chemical reactions often involving highly reactive oxygen intermediates (Thomas *et al* 1987), which produce direct or indirect cellular damage (Kessel *et al* 1998).

PDT is a superficial treatment characterized by a depth of necrosis, which depends on several parameters including delivered light dose, photosensitizer concentration and tissue optical properties. There have been many approaches taken to improve PDT efficacy. Some investigators have designed photosensitizers that preferentially accumulate in tumour cells (Hill *et al* 1992). Other investigators have focused on delivering precisely the most desirable light dose for particular systemic photosensitizer concentrations. Treatments, in this case, prescribe a fixed light dose for each organ. Such treatment schemes have drawbacks. For example, tissue optical properties, photosensitizer concentrations and ergo necrosis depths may vary throughout the treated organs. Clearly, knowledge about these parameters in treated areas can be used to optimize the delivered fluence rate and hence the treatment effect (Tromberg *et al* 1990, Foster and Gao 1992, Busch *et al* 2000).

In this work, we show how reflection-based broadband absorption spectroscopy may be used effectively *in situ* to determine tissue optical properties important for PDT dosimetry. We have developed algorithms, based on the diffusion approximation, to model photon transport in tissue and recover tissue optical properties from the reflectance measurements. Our instrumentation and analysis methods were validated in measurements of tissue-like, homogeneous Intralipid$^R$ phantoms. The instrument was then used *in vivo* to measure the uptake of a second-generation photosensitizer, MLu, as well as the optical properties, haemoglobin concentration and haemoglobin oxygen saturation in normal canine large bowels, prostates and kidneys. Such measurements provide feedback to clinicians that can be used to improve PDT treatment.

## 2. Materials and methods

### 2.1. Design of reflectance spectrometer

We have built a white-light absorption spectrometer to measure the wavelength-dependent reflectance of tissue simultaneously at many source–detector separations (figure 1(a)). This design is based on similar optical instruments that are described in the literature (Nichols *et al* 1997, Weersink *et al* 1997, Mayevsky *et al* 1988). Our probe uses a broadband fibre-optic-coupled light source. Light from a 150 W mercury arc lamp (Oriel) is coupled to the tissue through a 640 $\mu$m core diameter optical fibre (the source fibre). Approximately 100 $\mu$W of
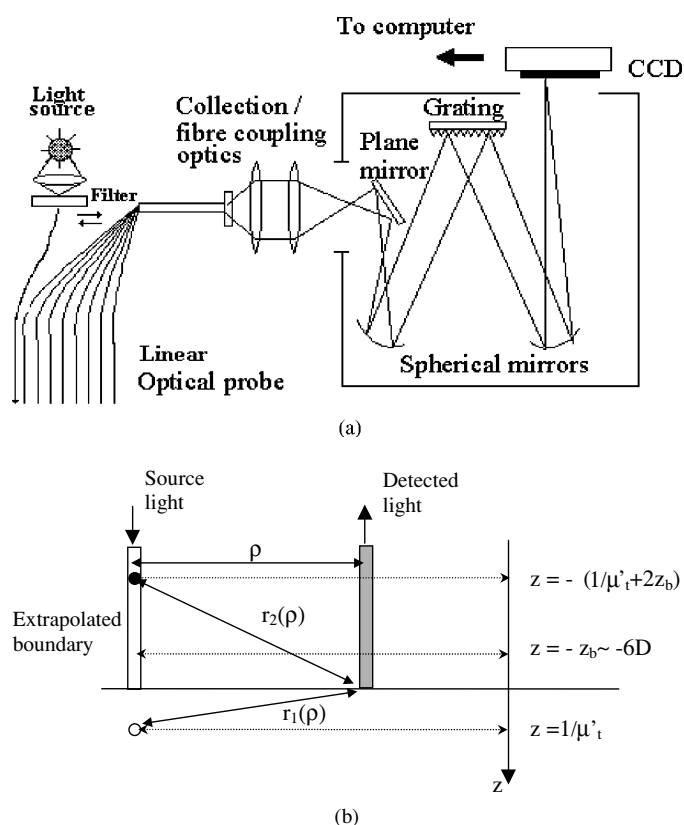
(a)



(b)

**Figure 1.** (a) Schematic of the experimental set-up for the continuous wave absorption measurements. The instrument consists of three major parts: the CCD camera, the dispersion system (monochromator) and the fibre-optic probe head. (b) Schematic of the experimental fibre configuration showing the relative positions of surface boundary, extrapolated boundary, $r_1(\rho)$ and $r_2(\rho)$ (Hull *et al* 1998). (c) Block diagram of the fitting procedure.

light derived from the lamp was coupled to the tissue in this way. Detection was accomplished using six optical (detection) fibres in a line, with 1 mm separation between adjacent fibres. The distance between the source and the first detection fibre was 1 mm. The use of many optical fibres provides high sensitivity, since it is possible to simultaneously measure small signal changes at large and small source–detector separations. We were thus able to measure haemoglobin absorption from reflectance spectra in the 700 nm region, which is sensitive to depths of order 5 mm (Jacques 1989) below the tissue surface.

The remitted light was transferred to the entrance slit of an imaging monochromator (300 g mm$^{-1}$, $f = 4$, Acton Research, Acton, MA). The monochromator output (i.e. image) plane contained six vertically spaced lines representing spectra corresponding to the six detection fibres. The reflectance spectra, $R_{\text{tissue}}(\rho, \lambda)$, were collected concurrently by a CCD camera (Princeton Instruments, 16 bit, liquid nitrogen cooled to 163 K, 24 $\mu$m pixel size, $330 \times 1100$ pixels). The CCD camera sensor was placed in the image plane of the monochromator, and the CCD pixels were binned across each 'detector' line.

To account for the background light signals scattered inside the monochromator, $S(\rho, \lambda)$, the area of the detector between the six 'detector' lines was binned as well. These background signals (derived from the space between detector lines) were then subtracted from the nearby

Input parameters: initial guesses for $\mu_s'$, $\mu_a$, $a$, $o$.

↓

Minimization of
$$R_{meas}(\rho,\lambda) - [aR(\rho;\mu_a,\mu_s') + o]$$
by finding optimum $a$, $o$, $\mu_s'$ and $\mu_a$ at 650 and 800 nm.

↓

**Sequential fit**

$\mu_s'$ and $\mu_a$; $a$ and $o$ fixed.

↓

Minimization of
$$R_{meas}(\rho,\lambda) - [aR(\rho;\mu_a,\mu_s') + o]$$
at discrete wavelengths between 650 and 800 nm

↓

$\mu_a^s(\lambda)$, $\mu_s^{s\prime}(\lambda)$

↓

**SVD**

Expansion of the input $\mu_a^s(\lambda)$ spectra into basis spectra, using SVD,
$$\mu_a^s(\lambda) = \sum_i c_i \varepsilon_i(\lambda) + \delta(\lambda)$$
and $\mu_s^{s\prime}(\lambda)$ fit by $\mu_s^{s\prime}(\lambda) = A\lambda^{-B}$ using LM fitting.

↓

$c_i$, A, B

↓

**Global optimization**

Minimization of the difference between $R_{meas}(\rho,\lambda)$ and $R_{comp}(\rho, c_i, A, B, a^{comp}, o^{comp} \lambda)$ for all $\lambda$
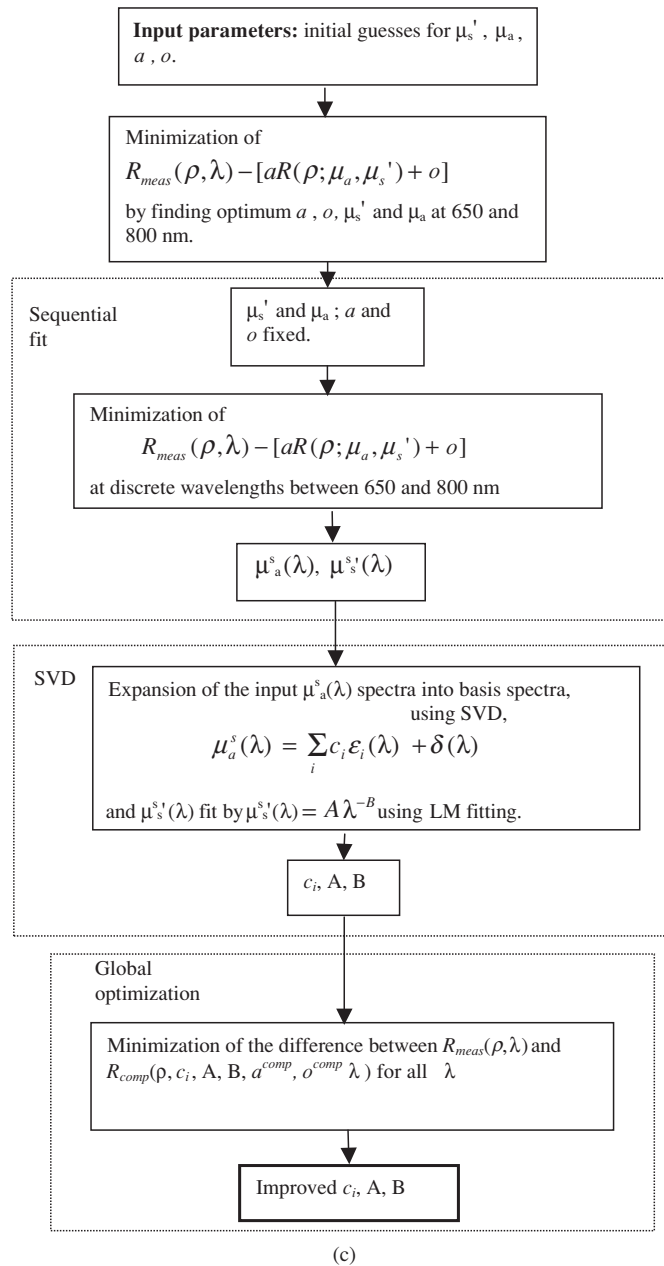
↓

Improved $c_i$, A, B

(c)

**Figure 1.** (Continued.)

measured signals, on a pixel-by-pixel basis for corresponding optical wavelengths. Typical signal integration times for measurements varied between 100 and 500 ms. Reflectance spectra were usually measured between 460 and 960 nm.

In order to account for variation in lamp intensity and the system response across the entire spectral region, an additional measurement was taken immediately before each experiment. The six-fibre optical probe was placed at the 0.5-inch opening of a 6-inch

diameter integrating sphere (LabSphere, Inc.); then the source light was turned on and a calibration signal $R_{\text{sphere}}(\rho, \lambda)$ was obtained for each of the detection fibres. The background subtraction as described above was performed using the data from the integrating sphere.

The effective measured reflectance, $R_{\text{meas}}(\rho, \lambda)$, was derived by dividing the background-subtracted tissue and integrating-sphere data pixel-by-pixel (i.e. at each optical wavelength):

$$R_{\text{meas}}(\rho, \lambda) = \frac{R_{\text{tissue}}(\rho, \lambda) - S^{\text{tissue}}(\rho, \lambda)}{R_{\text{sphere}}(\rho, \lambda) - S^{\text{sphere}}(\rho, \lambda)}. \tag{1}$$

Here $\rho$ is the distance between the source and detector fibres and $\lambda$ is the wavelength. (Note, we use $\rho$ to indicate the *specific source–detector pair* on the probe with separation $\rho$.) $R_{\text{tissue}}$ and $R_{\text{sphere}}$ represent the tissue and integrating-sphere reflectance signals and $S^{\text{tissue}}$, $S^{\text{sphere}}$ represent the corresponding background signals due to residual light scatter inside the instrument.

## 2.2. Multi-distance measurement algorithms

*In vivo* optical spectroscopy requires quantitative separation of tissue scattering effects, characterized by the scattering coefficient $\mu_s'$, from tissue absorption effects, characterized by the absorption coefficient $\mu_a$. In the near-infrared region ($\sim$800 nm), the photon transport mean free path is of the order of 1 mm (corresponding to a reduced scattering coefficient $\mu_s' = 10\,\text{cm}^{-1}$). This high degree of scattering tends to distort spectroscopic information because the large distribution of photon pathways through the tissue contributes to measured signals. Proper interpretation of our optical experiments requires an accurate theoretical model for light transport in tissue. The diffusion approximation is sufficient to model light transport for the present experiments. Using this basic physical model, one can accurately incorporate the effects of boundaries, such as the air–tissue interface, into the light transport theory (Patterson *et al* 1991). Solutions for uniform, highly-scattering semi-infinite media follow from the studies on light diffusion (Ishimaru 1978, Chance and Alfano 1995) and enable experimenters to extract the absorption and scattering coefficients of the underlying turbid medium (e.g. tissue) from position-dependent intensity measurements along the sample surface. The multi-distance approach is generally much less susceptible to systematic errors from superficial variations in skin absorption (Fantini *et al* 1994).

Diffusion theory for semi-infinite media predicts the reflectivity $R(\rho; \mu_a, \mu_s')$ for each source wavelength as a function of $\rho$, where $\rho$ is the source–detector separation along the sample surface. For our analysis, $R(\rho; \mu_a, \mu_s')$ is derived from photon flux and fluence rate at the boundary, as suggested in Farrell and Patterson (1992) and Hull *et al* (1998):

$$R(\rho; \mu_a, \mu_s') = C_1 \psi(\rho) + C_2 j_z(\rho) \tag{2}$$

where

$$\psi(\rho) = \frac{1}{4\pi D}\left(\frac{\exp(-\mu_{\text{eff}} r_1(\rho))}{r_1(\rho)} - \frac{\exp(-\mu_{\text{eff}} r_2(\rho))}{r_2(\rho)}\right) \tag{3a}$$

and

$$j_z(\rho) = \frac{1}{4\pi \mu_t'}\left[\left(\mu_{\text{eff}} + \frac{1}{r_1(\rho)}\right)\frac{\exp(-\mu_{\text{eff}} r_1(\rho))}{r_1^2(\rho)} + \left(\frac{1}{\mu_t'} + 2z_b\right)\left(\mu_{\text{eff}} + \frac{1}{r_2(\rho)}\right)\frac{\exp(-\mu_{\text{eff}} r_2(\rho))}{r_2^2(\rho)}\right]. \tag{3b}$$

Here, $\mu_t' = \mu_a + \mu_s'$ and $\mu_{\text{eff}} = [3\mu_a(\mu_a + \mu_s')]^{\frac{1}{2}}$. The photon diffusion coefficient is defined as $D = [3(\mu_a + \mu_s')]^{-1}$. $C_1$ and $C_2$ are constants that depend on the relative refractive index

mismatch between the tissue and the detector fibre, and the numerical aperture of the detection fibres[5]. The parameters $r_i(\rho)$ are defined in figure 1(b). Briefly, $r_1(\rho)$ is the distance from the point of contact of the detector fibre on the tissue surface to the effective source position in the tissue located $1/\mu'_t$ directly beneath the source fibre; $r_2(\rho)$ is the distance between the point of contact of the detector fibre and a point located $1/\mu'_t + 2z_b$ directly above the source. $z_b$ is the extrapolated boundary length above the surface of the medium (see figure 1(b)).

The absorption factor, $\mu_a$, depends on the chromophore concentrations and their extinction coefficients. The predominant absorbers in studied tissues are the photosensitizer, oxy-, deoxy-haemoglobin and water. The scattering factor depends on other tissue properties, such as organelle (e.g. mitochondria) concentration and the index of refraction of the background fluids. The reciprocal of the effective light attenuation coefficient, $\mu_{\text{eff}}$, is commonly used to define the depth of PDT light penetration. By measuring the absorption and scattering coefficients as a function of light wavelength, one generates a set of simultaneous equations that can be solved to yield the concentrations of the tissue chromophores. As alluded to earlier, information about chromophore concentrations and light penetration depth is useful for PDT dosimetry. Equations (2) and (3) have been validated by Monte Carlo simulation (Wang and Jacques 1995) and by us (data not shown).

## 2.3. Data analysis and algorithms

The data analysis and algorithms were developed using LabView[R] graphical programming language (National Instruments, Austin, TX). Extraction of tissue parameters from reflectance data is inherently challenging when the noise is not negligible. It was demonstrated (Hull *et al* 1998), however, that the Levenberg–Marquardt non-linear fitting routine is sufficient for the recovery of $\mu_a$ and $\mu'_s$ when the media are uniform, are well described by a semi-infinite model and when the signal-to-noise ratio is good (i.e. >30). Unfortunately, such conditions are rare for *in vivo* experiments.

Thus in our measurements, $\mu_a$ and $\mu'_s$ were extracted using a *three-step procedure*. *Step one* is a *sequential fit* (i.e. a sequence of fits at different optical wavelengths) that uses Boltzmann simulated annealing (BSA) to extract an initial estimate for $\mu_a(\lambda)$ and $\mu'_s(\lambda)$. *Step two* takes these initial estimates for $\mu_a(\lambda)$ and $\mu'_s(\lambda)$ and fits them to specific physical models incorporating known chromophores and a wavelength-dependent scattering function derived from Mie theory; the result of *step two* is an estimate of the principal chromophore concentrations ($c_i$) and two parameters ($A$, $B$) in the scattering theory. Finally, *step three* takes these estimates ($c_i$, $A$, $B$) and performs a global fit to all of the data in order to extract the best estimates of $c_i$, $A$, $i$ and ergo $\mu_a(\lambda)$ and $\mu'_s(\lambda)$; *step three* also employs the BSA algorithm. This entire process can be iterated, but we did not find iteration to be necessary. We describe these three steps in detail below (the interested reader may also wish to consult the flowchart in figure 1(c)).

In *step one* the reflectance data are sequentially fit using a BSA (Press 1992) routine at discrete wavelengths in the region of interest (typically between 650 and 800 nm, in steps of approximately 0.5 nm). In essence, for each wavelength we minimized

$$R_{\text{meas}}(\rho, \lambda) - [a R(\rho; \mu_a, \mu'_s) + o]. \qquad (4)$$

Here $a$ is a wavelength-independent scaling factor that matches amplitudes of measured and computed signals in the first fibre and $o$ is a wavelength-independent offset which is very small.

---

[5] $C_i = \dfrac{2i-1}{4\pi} \displaystyle\int_{\Omega_{\text{det}}} T_{\text{Fr}}(\theta) \cos^i \theta \, d\Omega$, $i = 1, 2$. Here, $T_{\text{Fr}}$ is the Fresnel transmission coefficient for unpolarized light that strikes the interface between the tissue and the detector at angle $\theta$ relative to the outward normal and $\Omega_{\text{det}}$ is the acceptance angle of the fibre. In the current paper, $C_1 = 0.0133$ and $C_2 = 0.039$.

Initial values of $\mu_a$, $\mu'_s$, $a$ and $o$ are obtained with the BSA routine and equation (4) using two wavelengths, 800 and 650 nm. These initial values of $a$ and $o$ are treated as fixed constants for the remainder of the *sequential fit*. We then determine $\mu_a$ and $\mu'_s$ at each wavelength using the BSA algorithm subject to two constraints: the scattering factor must be a decreasing function of wavelength and the product of $\mu_a$ and $\mu'_s$ must be related to the measured value of $\mu_{\text{eff}}$, i.e. $\mu_{\text{eff}} = (3\mu_a\mu'_s)^{\frac{1}{2}}$. The latter constraint is applied because at distances $\rho > 4/\mu'_s$, the reflectance at the tissue surface is well approximated as an exponential decay (Bolt and ten Bosch 1994), and so $\mu_{\text{eff}}$ is readily extracted from the experimental data.

At the conclusion of this first step (i.e. the sequential fit), we obtain preliminary estimates of $\mu^s_a(\lambda)$ and $\mu^{s\prime}_s(\lambda)$ from the reflection data. The superscript $s$ indicates that these estimates were derived from the *sequential fit*.

The second step of our algorithm has two independent parts, one for absorption and the other for scattering. In the case of absorption, we expand $\mu^s_a(\lambda)$ into a linear combination of components due to the different possible tissue chromophores (i.e. basis spectra) (Hull *et al* 1998), and then use singular value decomposition (SVD) techniques to extract the concentrations of the tissue chromophores. This procedure assumed that the photosensitizer, oxy-haemoglobin, deoxy-haemoglobin and water were the predominant chromophores in the spectral region of interest, i.e.

$$\mu^s_a(\lambda) = \sum_i c_i \varepsilon_i(\lambda) + \delta(\lambda). \tag{5a}$$

Here, $\varepsilon_i(\lambda)$ is molar spectral absorbance of the $i$th chromophore, the $c_i$ are fit parameters which ultimately represent the molar concentration of the major chromophores and $\delta(\lambda)$ is the background residue of SVD. Units of $c_i$ and $\varepsilon_i(\lambda)$ are chosen so that the unit of their product is (length)$^{-1}$. For MLu, for example, $\varepsilon_i(\lambda)$ represents absorptivity, in cm$^{-1}$ of 1 mg l$^{-1}$ drug solution and $c_i$ represents the drug concentration in mg l$^{-1}$. In the phantom measurements, $\delta(\lambda)/\mu^s_a(\lambda) < 0.02$. For the *in vivo* measurements, $\delta(\lambda)/\mu^s_a(\lambda) < 0.15$. The larger tissue residual arises because the tissue samples are not homogeneous semi-infinite media and because there can be some residual absorption due to other chromophores. Our assumption of four chromophores is supported by the absence of unexpected absorption peaks in the results of the sequential fit and by the relatively small values of $\delta(\lambda)$. After the fitting, we define a *revised* wavelength-dependent absorption coefficient, $\mu_a(\lambda) = \sum_i c_i \varepsilon_i(\lambda)$ using our best estimates of $c_i$.

The scattering part of *step two* is similar in spirit to the absorption approach. We assume $\mu^{s\prime}_s(\lambda)$ has the form

$$\mu^{s\prime}_s(\lambda) = A\lambda^{-B}. \tag{5b}$$

This form is an approximation that follows from the Mie theory (see, for example Doornbos 1999, Zonios 1999). We then use the LM non-linear fitting technique to determine the best estimate of $A$ and $B$. After the fitting, we define a *revised* wavelength-dependent scattering coefficient, $\mu'_s(\lambda)$, using our best estimates of $A$ and $B$ and equation (5b).

At the conclusion of the second step we have obtained good estimates of the four chromophore concentrations, $c_i$, *and the parameters in the scattering fit, A and B. We use this information as an initial guess for a final, global fit to the data.* In the *third step*, a wavelength-dependent computed reflectance, $R_{\text{comp}}$, is calculated using equation (2) and the *revised* scattering and absorption coefficients:

$$R_{\text{comp}}\left(\rho, c_i, a^{\text{comp}}, o^{\text{comp}}, A, B, \lambda \right. = a^{\text{comp}} R(\rho, \mu_a(\lambda), \mu'_s(\lambda)) + o^{\text{comp}}. \tag{6}$$

The parameters $a^{\text{comp}}$ and $o^{\text{comp}}$ have the same meaning as the parameters $a$ and $o$ in the first step. The computed reflectance, $R_{\text{comp}}$, thus depends on eight parameters (i.e., four $c_i$, $a^{\text{comp}}$, $o^{\text{comp}}$, $A$, $B$).

In order to determine the most likely values for the concentrations $c_i$, $A$ and $B$, the measured reflectance, $R_{\text{meas}}(\rho, \lambda)$, is now compared to $R_{\text{comp}}$. The following cost function, $\Xi$, is minimized globally for all $\rho$ and $\lambda$ using the BSA technique:

$$\Xi\left(c_i, a^{\text{comp}}, o^{\text{comp}}, A, B\right) = \frac{R_{\text{meas}}(\rho, \lambda) - R_{\text{comp}}\left(\rho, c_i, a^{\text{comp}}, o^{\text{comp}}, A, B, \lambda\right)}{R_{\text{meas}}(\rho, \lambda)} + \eta \zeta_{\mu_{\text{eff}}}$$

$$\zeta_{\mu_{\text{eff}}} = \frac{\mu_{\text{eff}}^{\text{refl}} - \mu_{\text{eff}}^{\text{comp}}}{\mu_{\text{eff}}^{\text{refl}}} \,.$$

(7)

Here, $\mu_{\text{eff}}^{\text{refl}}$ is determined from the experimental reflection data and $\mu_{\text{eff}}^{\text{comp}}$ is found from $R_{\text{comp}}$ at large source–detector separations (i.e., both values are estimated for $\rho > 4/\mu'_s$). The constant $\eta$ represents a penalty coefficient for the mismatch between $\mu_{\text{eff}}$ of the measured and computed reflectance; it was empirically set to 0.25 based on phantom measurements. This form for the cost function (equation (7)) was found experimentally to provide better convergence than the traditional $\chi^2$ form.

As a result of the minimization of (7), the values of $c_i$, $A$ and $B$ from step 2 were improved. Thus steps 1 and 2 serve as a pre-processing scheme, supplying the main fitting routine (step 3) with a good initial guess. Taken together, our algorithm differs significantly from popular techniques that rely on a high-quality initial guess.

### 2.4. Tissue phantoms

Tissue phantoms were prepared from Intralipid® 10% as the turbid medium. Intralipid is an emulsion made mostly of water and soyabean oil. It is a polydisperse suspension of droplets with an average diameter of $\sim$0.4 $\mu$m (and range from 0.1 to 1.0 $\mu$m) (van Staveren *et al* 1991). The reduced scattering coefficient, $\mu'_s$, of the phantom was varied by changing the water content of the Intralipid. The absorption of MLu® was modelled by adding the photosensitizer in amounts of 0.33, 0.67, 1.33 and 2.67 mg l$^{-1}$ to the Intralipid phantoms.

### 2.5. Motexafin lutetium

MLu (Young *et al* 1996) was supplied as a 2 mg ml$^{-1}$ aqueous solution by Pharmacyclics, Inc. (Sunnyvale, CA). The solution was stored in a refrigerator and protected from light. The MLu solution was injected into the cephalic vein of three dogs during a period of 5 to10 min, via a 20 gauge intravenous catheter. The volume administered to each animal was based on the weight of each dog and the target dose level in mg kg$^{-1}$.

### 2.6. Photodynamic treatment conditions

Four dogs (laboratory Beagles) ranging in age from 8 to 17 months and weighing 9.0–23.6 kg were used in this study. The animals were housed according to the Guide for the Care and Use of Laboratory Animals, National Academy Press, Washington, DC 1996. Animals were cared under the supervision of veterinarians from the University of Pennsylvania, School of Veterinary Medicine. The experimental protocol was approved by the University of Pennsylvania Institutional Animal Care and Use Committee.

MLu was administered intravenously $3 \pm 0.5$ h before light delivery. This drug-light interval was chosen because in pre-clinical models, 3 h was associated with maximal efficacy (Woodburn *et al* 1997) and because 3–5 h was used initially for the phase I human clinical trial of MLu (Yuen *et al* 1997). The dogs were anaesthetized with 10 mg kg$^{-1}$ intravenously (IV) thiopental sodium (Abbott Laboratories, North Chicago, IL) and intubated with an

endotracheal tube (Rusch, Germany). General anaesthesia was maintained with an inhaled mixture of oxygen and isoflurane. During surgery, animals received a constant IV infusion of Normosol-R (Abbott Laboratories, North Chicago, IL) at a rate of 20 ml/kg/h. Cefazolin sodium, 20 mg kg$^{-1}$, (Marsam Pharmaceuticals, Inc., Cherry Hill, NJ) was administered IV every 2 h during the surgical procedure. While under anaesthesia, ECG tracings, blood pressure and oxygen saturation were continuously monitored. The dogs subsequently underwent a laparotomy to expose the entire abdominal contents. PDT light was delivered to the exposed organs. The results of this pre-clinical trial have been reported elsewhere (Griffin *et al* 2001). Reflectance measurements were done before and after PDT.

Laser light for PDT was derived from a Diomed diode laser (Diomed, Cambridge, UK). One dog served as a light-only (no photosensitizer) control receiving the dose of 2 J cm$^{-2}$ at 730 nm.[6] The other three dogs were treated with MLu (2 mg kg$^{-1}$) and 0.5 J cm$^{-2}$ of 730 nm light (Griffin *et al* 2001). The average light fluence rate was $\leqslant$150 mW cm$^{-2}$, usually considerably lower. Protective filters were not placed over the operating room lights, which were dimmed during the treatment. The estimated dose at 730 nm from the dimmed surgical lights during treatment was less than 1% of the treatment exposure and did not affect the treatment results.

## 3. Results

We first used our instrument to study tissue phantoms. Then we performed *in vivo* measurements of tissue blood oxygen saturation, haemoglobin concentration, drug concentration and tissue scattering in the dog models. Finally, we explored how these parameters were changed by PDT treatment.

### 3.1. Validation with tissue phantoms

We confirmed the accuracy of our fitting routines using Intralipid phantoms, with and without MLu. The scattering coefficients were calibrated independently using our 1% Intralipid solutions at 630 nm. In particular, we compared the diffuse transmission of 1 cm wide Intralipid-filled slabs with the transmission of similar slabs filled with a water suspension of 400 $\mu$m diameter polystyrene spheres. The Mie theory was used to calculate $\mu'_s$ of the polystyrene sphere suspension and the diffusion theory was used to extract $\mu'_s$ from the transmission data (see, for example, Star 1989).

Published values of the reduced scattering coefficient of Intralipid 10% at 630 nm vary between $60 \pm 10$ cm$^{-1}$ (Flock *et al* 1992) and $130 \pm 7$ cm$^{-1}$ (van Staveren *et al* 1991). In the absence of significant inter-particle interactions, analogous numbers for Intralipid 1% should scale with concentration. The reduced scattering coefficient for 1% Intralipid at 630 nm was measured to be $10.7 \pm 0.5$ cm$^{-1}$ and for 2% Intralipid $\mu'_s$ was measured to be $21.0 \pm 0.8$ cm$^{-1}$. These values are consistent with scaled previous measurements of 10% Intralipid and so served as standards for $\mu'_s$ in the Intralipid phantom measurements discussed below.

Figure 2 shows the recovery of scattering and absorption spectra from a phantom measurement. Since the Intralipid emulsion is 99% water, its $\mu_a$ is expected to be essentially that of water (Flock *et al* 1992). Both 1 and 2% Intralipid gave the correct absorption spectrum of water even at very small absorptions (i.e. of order $10^{-3}$ cm$^{-1}$). The recovered reduced scattering coefficient at 630 nm was also within a few per cent of the 'golden standard' value obtained using the slab geometry technique.

---

[6] In the larger study of which this paper is a part, the treated dogs were given a range of light doses, but controls were set at the highest values (2 J cm$^{-2}$) in order to reduce animal sacrifice.
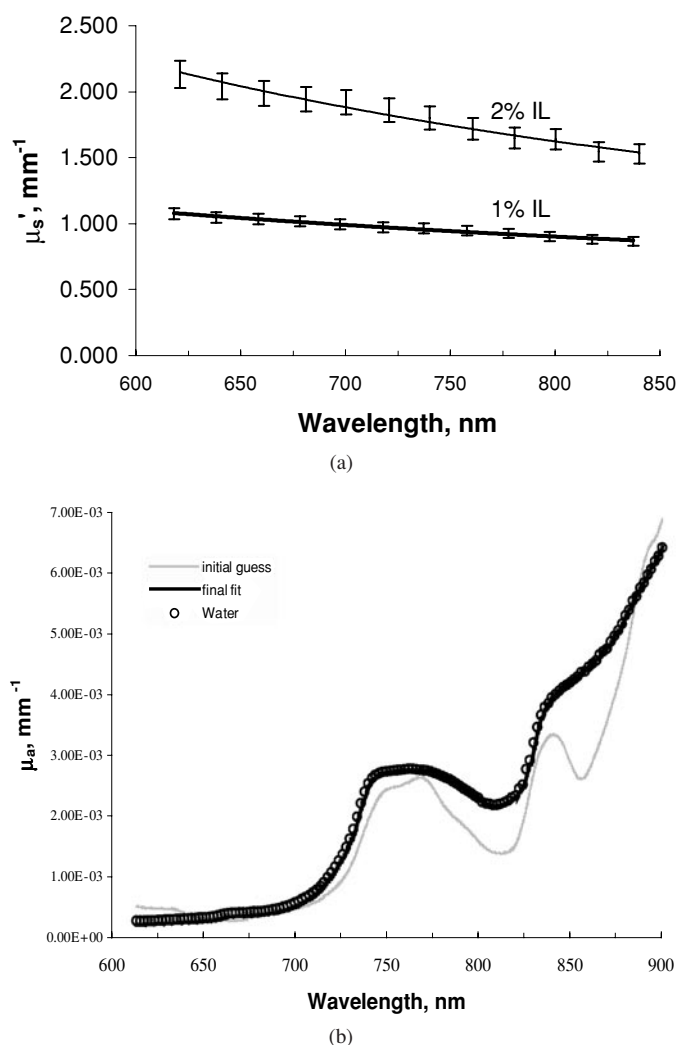
(a)



(b)

**Figure 2.** (a) Sample recovery (fits) of reduced scattering coefficients. The $\mu_s'(\lambda)$ obtained by sequential fit is approximated by a power law. Error bars are centred about the averaged sequential fit data and represent the measurement standard deviation. (b) Absorption spectra of 1% Intralipid phantom without MLu. (c) Absorption spectra of 1% Intralipid phantom with MLu. (d) The average recovered values (together with standard deviations in brackets) of MLu concentration at 0.33, 0.67, 1.33 and 2.67 mg l$^{-1}$ and the corresponding linear fit of recovered concentrations. The recovered concentrations were, respectively: 0.443 (0.095), 0.659 (0.039), 1.26 (0.066) and 2.92 (0.40) mg l$^{-1}$.

A comparison of the known water absorption spectra with our recovered spectra is presented in figure 2(b). The dotted line shows the results of our initial (step 1) sequential fit; note, the fitted $\mu_a$ is close to the literature values of water (**Kou** *et al* 1993, **Pope and Fry** 1997) at short wavelengths, but as the wavelength increases our recovered $\mu_a$ diverges somewhat with respect to the literature $\mu_a$. This deviation with increasing wavelength has also been noted by other investigators (**Hull** *et al* 1998). The recovery of $\mu_a$ improves substantially with further processing steps, i.e. the SVD and global minimization procedures. During the SVD
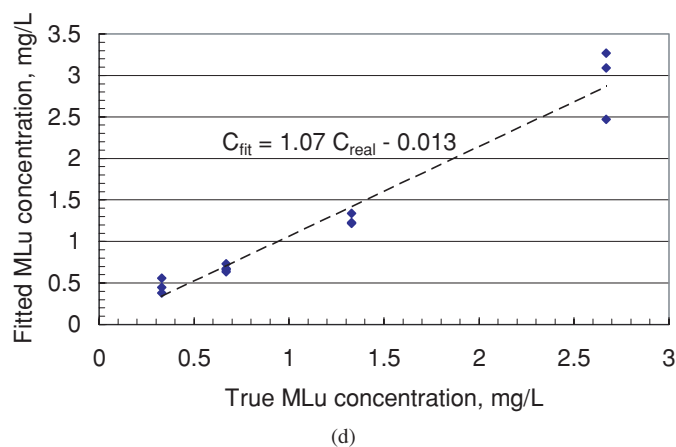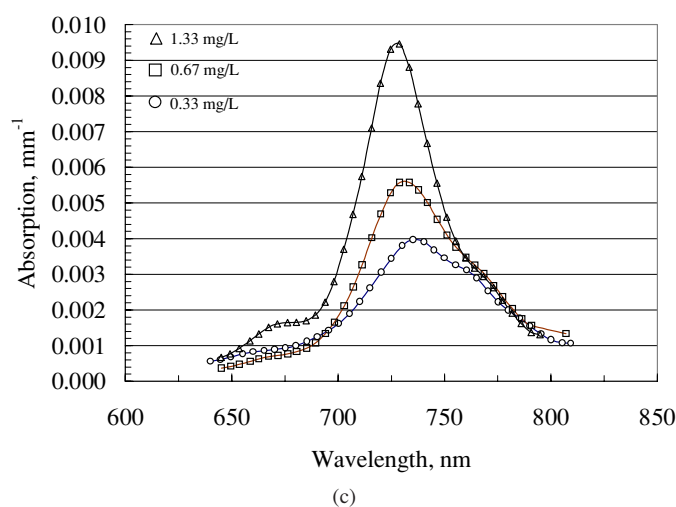
(c)



(d)

**Figure 2.** (Continued.)

step, the spectrum was fitted with one chromophore (water) and constant offset. After global minimization, $\mu_a$ was within 3% of the literature water absorption spectrum.

The calculated variation of $\mu'_s$ with wavelength over the same spectral range is given in figure 2(a). As follows from the Mie theory (Saidi *et al* 1995), $\mu'_s$ decreased with increasing wavelength. The $\mu'_s$ of 1% Intralipid was well approximated by a function of the form, $\mu'_s = 1.41\lambda^{-0.758}$ (with correlation coefficient $R^2 = 0.98$). The measured value of $\mu'_s$ of 2% Intralipid was also about twice that of 1% Intralipid, as expected.

Figures 2(c) and (d) exhibit data from the same tissue phantoms with added photosensitizer. The data clearly demonstrate concentration linearity in the recovery of absorption for 0.33, 0.67 and 1.33 mg l$^{-1}$ MLu in 1% Intralipid. The MLu absorption peaked at approximately 737 nm. In the absence of background scatter, the accuracy of the recovery ranged from 35 (for 0.33 mg l$^{-1}$) to 8% (for 1.33 mg l$^{-1}$). (Here, accuracy corresponds to the 95% confidence interval based on four consecutive independent measurements under the same experimental conditions.) The large recovery error for 0.33 mg l$^{-1}$ of MLu was because this MLu concentration was close to our detection limit. Note also that the recovered $\mu'_s(\lambda)$ of the

phantoms containing MLu were nearly identical to those of the MLu-free 1 and 2% Intralipid phantoms. This demonstrates an absence of coupling between recovered $\mu_a(\lambda)$ and $\mu'_s(\lambda)$.

The tissue phantom experiments validate our method of absorption and scattering recovery in ideal samples. The measurements also suggest that we now have a robust and viable tool to investigate the concentration of chromophores in tissues.

### 3.2. In vivo measurements

Next, we obtained *in vivo* measurements of tissue optical properties, oxygenation and photosensitizer concentration before and after PDT in dogs. The second-generation photosensitizer MLu has been used at the Hospital of the University of Pennsylvania in clinical trials for treatment of recurrent breast and prostate cancers. The primary goal of the study on beagle dogs described herein, was to evaluate the toxicity of MLu-mediated intraperitoneal PDT; the secondary goal of the study was to collect baseline optical information on canine large bowels, prostates and kidneys and test our instrumentation *in vivo*.

*3.2.1. Photosensitizer concentrations.* All our analysis assumed that the tissues of interest were semi-infinite homogeneous media and the light transport through these media was well approximated as a diffusion process. We further assumed that oxy-haemoglobin, deoxy-haemoglobin, water and MLu were the major chromophores in the spectral region of 650 to 800 nm in canine tissues. An example of typical *in vivo* reflectance spectra for canine large bowels, kidneys and prostates is exhibited in figure 3(a). The dip at 740 nm corresponds to the MLu absorption. Using the analysis method outlined earlier (e.g., equations (5*a*), etc.), the concentrations of MLu, oxy-haemoglobin and deoxy-haemoglobin were calculated from the reflectance data. The extinction coefficient of water, $\varepsilon_{H_2O}(\lambda)$, was taken from previous reports (Kou *et al* 1993, Pope and Fry 1997). The haemoglobin extinction coefficients, $\varepsilon_{HbO_2}(\lambda)$ and $\varepsilon_{Hb}(\lambda)$, were taken from the compilation spectra prepared by Scott Prahl (http://omlc.ogi.edu/spectra/haemoglobin/index.html). The extinction coefficient of 1 mg l$^{-1}$ of MLu, $\varepsilon_L(\lambda)$, was obtained from previous reports (Kostenich *et al* 1998, Young *et al* 1996). The coefficients $c_{H_2O}$, $c_L$, $c_{HbO_2}$ and $c_{Hb}$ are correspondingly the concentrations of water, MLu (mg kg$^{-1}$), oxyhaemoglobin and deoxyhaemoglobin (mM). The fitting was performed between 690 and 810 nm.

*3.2.2. Tissue optical properties: scattering, MLu absorption, light penetration.* The wavelength dependence of the reduced scattering coefficient, $\mu'_s(\lambda)$, was different for various organs. The best fits yielded the following: $\mu'_s(\lambda) = 3667\lambda^{-1.24}$ for large bowel, $\mu'_s(\lambda) = 41719\lambda^{-1.51}$ for kidney and $\mu'_s(\lambda) = 411\lambda^{-0.876}$ for prostate. Here, $\lambda$ is in nanometres and $\mu'_s(\lambda)$ in mm$^{-1}$. At the clinically important wavelength of 730 nm, the mean values of $\mu'_s(\lambda)$ ($\pm$SD) for large bowel, kidney and prostate were: $10.1 \pm 1.3$ cm$^{-1}$, $19.6 \pm 4$ cm$^{-1}$ and $12.7 \pm 0.6$ cm$^{-1}$, respectively. We also found that the absorption of MLu at 730 nm was strong enough to influence the optical properties of tissues; that is the penetration depth of the treatment light in tissue decreased due to photosensitizer absorption. This is shown in table 1, where the photosensitizer-induced changes of $\mu_{\text{eff}}$ at 730 nm are shown. In the case of large bowel, MLu absorption was found to decrease light penetration by ~50% (see table 1). Since effective penetration depth is the major determinant of the PDT efficacy, it is desirable to consider this class of effects in computations of desired threshold dose.
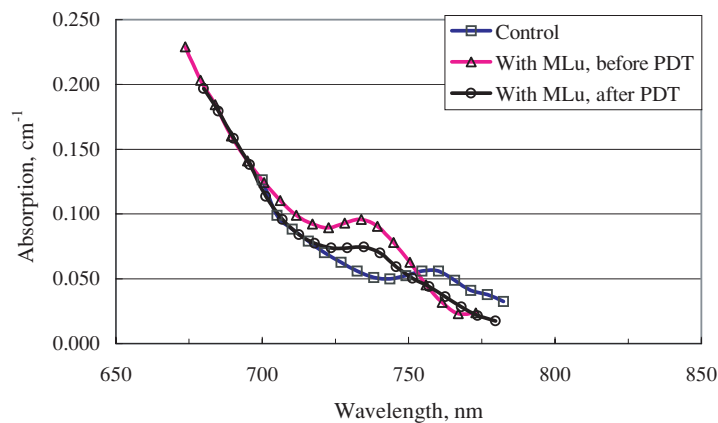
Examples of the reconstructed and measured reflectance are shown in figure 3(a). Measurements were typically performed at three locations on each organ of each dog. After the injection of 2 mg kg$^{-1}$ MLu, the tissue MLu concentration was found to be (mg l$^{-1}$,
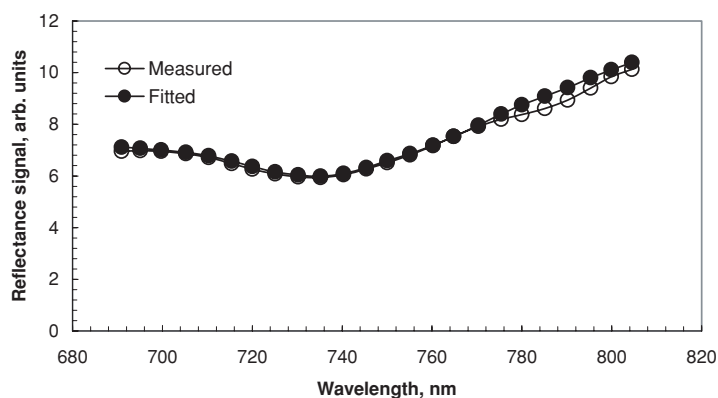
(a)
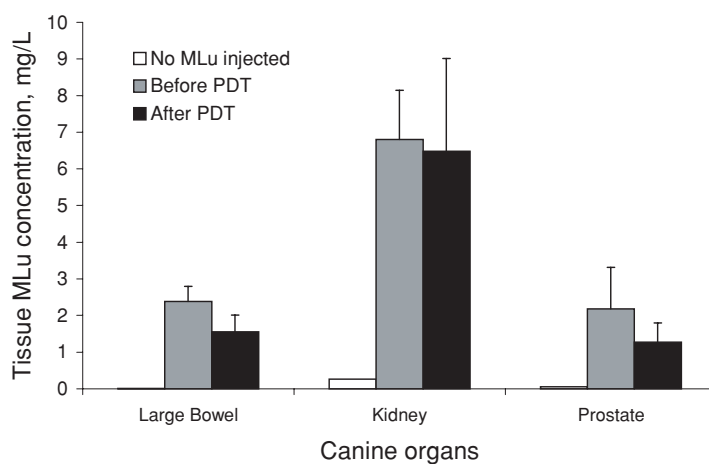


(b)



(c)

**Figure 3.** (a) Reflectance and fit of a large bowel measurement before PDT, $\rho = 3$ mm. (b) Tissue MLu concentration before and after PDT. (c) Absorption spectra (sequential fit results) of canine large bowel (control, before and immediately after PDT). The data presented were averaged over three animals and one control, three measurements on each.

**Table 1.** Effective attenuation coefficients for canine organs obtained *in vivo* before and after PDT. For each organ, Lutex data were averaged over three dogs, three measurements on each. Additionally, one dog was used as control.

| Organ | $\mu_{\text{eff}}$ at 730 nm, cm$^{-1}$ | | | | | |
|---|---|---|---|---|---|---|
| | Kidneys | | Large bowels | | Prostates | |
| | Before PDT | After PDT | Before PDT | After PDT | Before PDT | After PDT |
| Control | 5.25 | 4.51 | 1.25 | 1.04 | 2.05 | 1.82 |
| With MLu, 2 mg kg$^{-1}$ | 6.74 | 6.05 | 2.43 | 2.34 | 2.70 | 2.18 |
| Standard Deviation | 1.1 | 0.62 | 0.30 | 0.41 | 0.36 | 0.22 |

standard deviation): 2.4 (0.4) for large bowel, 6.8 (1.3) for kidney and 2.2 (1.1) for prostate. We observed significant variability in MLu uptake among the organs and in the same organs of different dogs. The variability of MLu concentration between different measurements on the same organ of a dog was about 20–30%. The variability among the same organ in different animals ranged from 20 to 40%. The MLu concentration in kidneys was 2–3 times that of large bowels and prostates (figure 3(b)). This result is reasonable, since the primary route for drug clearance is through the kidneys.

It is known that the combination of light and drug dose is related to PDT tissue and tumour destruction (Hill *et al* 1995). The high variablity of MLu uptake among the canine organs suggests that the light dose to a specific organ may need to be adjusted to account for the actual tissue uptake of MLu.

Photobleaching of photosensitizers during PDT has been previously studied (Kessel 1990, Robinson *et al* 1998). In our study, we found a statistically borderline decrease in the MLu absorption of large bowels and prostates after light treatment (figures 3(b) and (c), table 1). This might suggest that photobleaching of MLu is present even when the delivered light dose is relatively low (0.5 J cm$^{-2}$ at 730 nm). Therefore, it might be desirable to account for the photobleaching of MLu during treatment planning for PDT.

*3.2.3. Tissue oxygenation and haemoglobin.* Figure 4(a) exhibits the measured oxygen saturation (i.e. $c_{\text{HbO}_2}/(c_{\text{Hb}} + c_{\text{HbO}_2}) \times 100$) for large bowel, kidney and prostate. No statistically significant difference in haemoglobin oxygen saturation was observed between the control and the MLu-injected dogs for the sample size of the conducted experiments. Immediately after light delivery with 0.5 J cm$^{-2}$, 730 nm light at 150 mW cm$^{-2}$, the oxygen saturation was unchanged, at least within the accuracy of the measurements. The mean (standard deviation) haemoglobin concentrations of large bowels, kidneys and prostates, of all control and MLu-injected dogs were found to be, respectively, 119 (25), 340 (92) and 51 (11) $\mu$M (figure 4(b)).

Oxygen is one of the main ingredients of PDT and has been found to be consumed during PDT (Henderson and Dougherty 1992, Doornbos *et al* 1999). Haemoglobin oxygen saturation was fairly similar among the organs. Similar levels of oxygenation (i.e. $\sim$70%) were also found in human colon using another variant of reflectance spectroscopy (Zonios *et al* 1999). In our study, however, statistically significant changes in tissue blood oxygenation before and after PDT treatment were not observed (figure 3(c)). This might be partly due to the small sample size used in this study, or it could be due to the relatively low fluences used in this study.
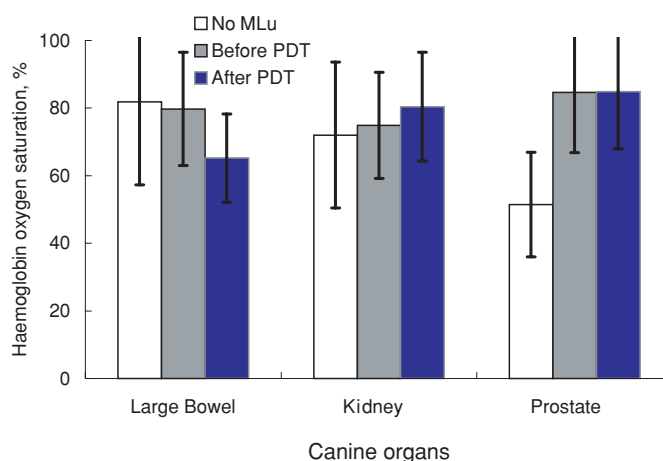
(a)
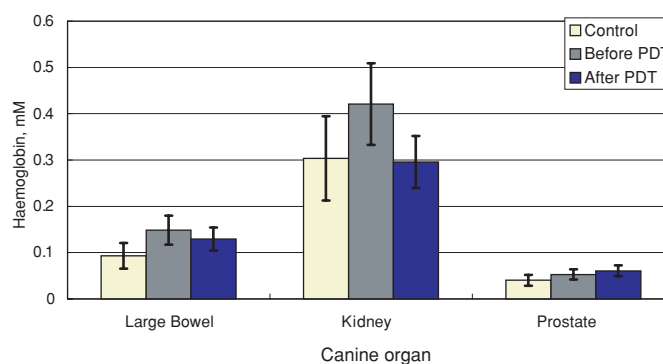


(b)

**Figure 4.** (a) Results of *in vivo* measurement of tissue oxygenation in canine large bowels, kidneys and prostates. (b) *In vivo* measurement of tissue total haemoglobin concentrations for different organs.

## 4. Conclusions

Models for photodynamic dosimetry (Patterson *et al* 1990, van Gemert *et al* 1985, Farrell *et al* 1998 and others, Lilge *et al* 1996) offer a quantitative basis for the improvement of PDT treatment protocols and require accurate measurements of tissue optical properties for their implementation. Instruments and algorithms for rapid *in situ* measurement and extraction of *in vivo* tissue optical properties non-invasively are important for the future individualization of PDT dosimetry. In this paper we have demonstrated such a device and have obtained data from animal models relevant to PDT. We have observed significant variability in MLu uptake among normal canine tissues. Thus *in situ* measurements of MLu uptake during PDT treatment may be necessary to individualize PDT drug and light delivery. Our data suggest that PDT light dosimetry may need to be tailored by patient, organ and local tissue physiology. In view of the significant variations in $\mu_a$ and $\mu_s'$ reported in this paper, PDT treatment individualization may be a useful approach.

## Acknowledgments

## References

Bolt and ten Bosch1994 On the determination of optical parameters for turbid materials *Waves Turbid Media* **4** 233–42

Busch T M, Hahn S M, Evans S M and Koch C J 2000 Depletion of tumor oxygenation during photodynamic therapy: detection by the hypoxia marker EF3 [2-(2-nitroimidazol-1[H]-yl)-*N*-(3,3,3-trifluoropropyl)acetamide] *Cancer Res.* **60** 2636–42

Chance B and Alfano R R 1995 *Proc. Optical Tomography, Photon Migration, and Spectroscopy of Tissue and Model Media: Theory, Human Studies, and Instrumentation* SPIE vol. I, II.

Doornbos R M P, Lang R, Aalders M C, Cross F W and Sterenborg H J C M 1999 The determination of *in vivo* human tissue optical properties and absolute chromophore concentrations using spatially resolved steady-state diffuse reflectance spectroscopy *Phys. Med. Biol.* **44** 967–81

Dougherty T J, Gomer C J, Henderson B W, Jori G, Kessel D, Korbelik M, Moan J and Peng Q 1998 Photodynamic therapy *J. Natl. Cancer Inst.* **90** 889–905

Fantini S, Franceschini M A, Maier J S, Walker S and Gratton E 1994 Frequency domain multi-source optical spectrometer and oximeter *Proc. SPIE* **2326** 108–16

Farrell T J and Patterson M S 1992 A diffusion theory model of spatially resolved, steady-state diffuse reflectance for the noninvasive determination of tissue optical properties *in vivo Med. Phys.* **19** 879–88

Farrell T J, Wilson B C, Patterson M S and Olivo M C 1998 Comparison of the *in vivo* photodynamic threshold dose for photofrin, mono- and tetrasulfonated aluminum phthalocyanine using a rat liver model *Photochem. Photobiol.* **68** 394–9

Flock S T, Jacques S L, Wilson B C, Star W M and van Gemert M J 1992 Optical properties of Intralipid: a phantom medium for light propagation studies *Lasers Surg. Med.* **12** 510–9

Foster T H and Gao L 1992 Dosimetry in photodynamic therapy: oxygen and the critical importance of capillary density *Radiat. Res.* **130** 379-83

Griffin G M, Zhu T, Solonenko M, DelPiero F, Kapatkin A, Busch T M, Yodh A, Polin G, Bauer T, Fraker D and Hahn S M 2001 Preclinical evaluation of motexafin lutetium-mediated intraperitoneal photodynamic therapy in a canine model *Clin. Cancer Res.* **7** 374–81

Henderson B W and Dougherty T J 1992 How does photodynamic therapy work? *Photochem. Photobiol.* **55** 145–57

Hill J S, Kahl S B, Kaye A H, Stylli S S, Koo M S, Gonzales M F, Vardaxis N J and Johnson C I 1992 Selective tumor uptake of a boronated porphyrin in an animal model of cerebral glioma *Proc. Natl. Acad. Sci. USA* **89** 1785–9

Hill J S, Kahl S B, Stylli S S, Nakamura Y, Koo M S and Kaye A H 1995 Selective tumor kill of cerebral glioma by photodynamic therapy using a boronated porphyrin photosensitizer *Proc. Natl. Acad. Sci.USA* **92** 1212–30

Hull E L, Nichols M G and Foster T H 1998 Quantitative broadband near-infrared spectroscopy of tissue-simulating phantoms containing erythrocytes *Phys. Med. Biol.* **43** 3381–404

Ishimaru A 1978 *Wave Propagation and Scattering in Random Media* vol 1 (New York: Academic)

Jacques S L 1989 Simple theory, measurements, and rules of thumb for dosimetry during photodynamic therapy *SPIE Proc. Photodynamic Therapy: Mechanisms* ed T J Dougherty vol. 1065 p 100

Kessel D 1990 *Photodynamic Therapy of Neoplastic Disease* vol 1, 2 (Boca Raton, FL: CRC Press)

Kessel D, Hampton J, Fingar V and Morgan A 1998 Tumor versus vascular photodamage in a rat tumor model *J. Photochem. Photobiol. B* **45** 25–7

Kostenich G, Orenstein A, Malik Z and Ehrenberg B 1998 *Preclinical Photodynamic Therapy Studies with Endogenous and New Exogenous Photosensitizers. Photodynamic Tumor Therapy: 2nd and 3rd Generation Photosensitizers* (Amsterdam: Harwood Academic)

Kou L, Labrie D and Chylek P 1993 Refractive indices of water and ice in the 0.65 to 2.5 mm spectral range *Appl. Opt.* **32** 3531–3540

Lilge L, Olivo M C, Schatz S W, MaGuire J A, Patterson M S and Wilson B C 1996 The sensitivity of normal brain and intracranially implanted VX2 tumour to interstitial photodynamic therapy *Br. J. Cancer* **73** 332–43

Liu H, Boas D A, Zhang Y, Yodh A G and Chance B 1995 Determination of optical properties and blood oxygenation in tissue using continuous NIR light *Phys. Med. Biol.* **40** 1983–93

Mayevsky A, Nioka S and Chance B 1988 Fiber optic surface fluorimetry/reflectometry and 31-p-NMR for monitoring the intracellular energy state *in vivo Adv. Exp. Med. Biol.* **222** 365–74

Nichols M G, Hull E L and Foster T H 1997 Design and testing of a white-light, steady-state diffuse reflectance spectrometer for determination of optical properties of highly scattering systems *Appl. Opt.* **36** 93–104

Patterson M S, Moulton J D, Wilson B C, Berndt K W and Lakowicz J R 1991 Frequency domain reflectance for the determination of the scattering and absorption properties of tissues *Appl. Opt.* **30** 44–74

Patterson M S, Wilson B C and Graff R 1990 *In vivo* tests of the concept of photodynamic threshold dose in normal rat liver photosensitized by aluminum chlorosulphonated phthalocyanine *Photochem. Photobiol.* **51** 343–9

Pope R M and Fry E S 1997 Absorption spectrum (380–700 nm) of pure water. II. Integrating cavity measurements *Appl. Opt.* **36** 8710–23

Press W 1992 *Numerical Recipes in C: The Art of Scientific Computing* (Cambridge: Cambridge University Press)

Robinson D J, de Bruijn H S, van der Veen N, Stringer M R, Brown S B and Star W M 1998 Fluorescence photobleaching of ALA-induced protoporphyrin IX during photodynamic therapy of normal hairless mouse skin: the effect of light dose and irradiance and the resulting biological effect *Photochem. Photobiol.* **67** 140–9

Saidi I S, Jacques S L and Tittel F K 1995 Mie and Rayleigh modeling of visible-light scattering in neonatal skin *Appl. Opt.* **34** 7410–18

Star W M 1989 Comparing P3-approximation with diffusion theory and with Monte-Carlo calculations of light propagation in a slab geometry *SPIE Inst. Ser.* **IS5** 146–54

Thomas J P, Hall R D and Girotti A W 1987 Singlet oxygen intermediacy in the photodynamic action of membrane-bound hematoporphyrin derivative *Cancer Lett.* **35** 295–302

Tromberg B J, Orenstein A, Kimel S, Barker S J, Hyatt J, Nelson J S and Berns M W 1990 *In vivo* tumor oxygen tension measurements for the evaluation of the efficiency of photodynamic therapy *Photochem. Photobiol.* **52** 375–85

van Gemert J C, Berenbaum M C and Gijsberg G H M 1985 Wavelength and light dose dependence in tumor phototherapy with haematoporphyrin derivative *Br. J. Cancer* **52** 43–49

van Staveren H G, Moes C J M, van Marle J, Prahl S A and van Gemert M J C 1991 Light scattering in Intralipid-10% in the wavelength range of 400–1100 nm *Appl. Opt.* **30** 4507–14

Wang L-H and Jacques S L 1995 MCML: Monte Carlo modeling of photon transport in multi-layered tissues *Comput. Methods Programs Biomed.* **47** 131–46

Weersink R A, Hayward J E, Diamond K R and Patterson M S 1997 Accuracy of noninvasive *in vivo* measurements of photosensitizer uptake based on a diffusion model of reflectance spectroscopy *Photochem. Photobiol.* **66** 326–35

Woodburn K W, Fan Q, Miles D R, Kessel D, Luo Y and Young S W 1997 Localization and efficacy analysis of the phototherapeutic lutetium texaphyrin (PCI-0123) in the murine EMT6 sarcoma model *Photochem. Photobiol.* **65** 410–5

Young S W, Woodburn K, Wright M, Mody T D, Dow W C, Qing F, Sessler J and Miller R A 1996 Lutetium texaphyrin (PCI-0123): a near-infrared water soluble photosensitizer *Photochem. Photobiol.* **63** 892–7

Yuen A R, Panella T J, Wieman T J, Julius C, Panjehpour M, Taber S, Fingar V, Horning S J, Miller R A, Young S W and Renschler M F 1997 Phase I trial of photodynamic therapy with lutetium-texaphyrin *Proc. Am. Soc. Clin. Oncol.* vol 16, p 7685

Zonios G, Perelman L T, Backman V, Manoharan R, Fitzmaurice M, Van Dam J and Feld M S 1999 Diffuse reflectance spectroscopy of human adenomatous colon polyps *in vivo* *Appl. Opt.* **38** 6628–37